Received: 27 April 2020 | Revised: 2 October 2020 | Accepted: 12 November 2020

IET Microwaves, Antennas & Propagation

DOI: 10.1049/mia2.12078

ORIGINAL RESEARCH PAPER

Active reflection coefficients characterization system for multiple input multiple output antennas

Marina Jordão[1] | Daniel Belo[1] | Rafael F. S. Caldeirinha[2] | Arnaldo S. R. Oliveira[1] | Nuno B. Carvalho[1]

[1]Instituto de Telecomunicações e Departamento de Eletrónica, Telecomunicações e Informática, Universidade de Aveiro, Aveiro, Portugal

[2]Instituto de Telecomunicações and Polytechnic Institute of Leiria, Leiria, Portugal

Correspondence

Marina Jordão
Instituto de Telecomunicações e Departamento de Eletrónica, Telecomunicações e Informática, Universidade de Aveiro, Aveiro, 3810-193, Portugal.
Email: marinajordao@ua.pt

Funding information

Fundação para a Ciência e a Tecnologia, Grant/Award Number: SFRH/BD/143204/2019; Fundação para a Ciência e a Tecnologia, Grant/Award Number: SFRH/BD/142403/2018

Abstract

The main objective of this study is to present a characterization system that can be used to measure the active reflection coefficient of each port of the multiple input multiple output (MIMO) antennas, when the main beam is steered to an intended direction. Since MIMO systems are composed of antennas with several elements and each antenna element is connected to a power amplifier, an active component, the beamforming will contribute to the mismatch of each branch. To this extent, a calibrated measurement system has been implemented using off-the-shelf software defined radio and designed to effectively extract such coefficients, when all the ports are simultaneously excited. Results for linear and planar MIMO antenna arrays have been experimentally obtained for several beam directions and the impact of beamforming on each element of the antenna is presented and compared to simulated results. Additionally, their behaviour was also assessed when some of the radiation elements are deliberately disconnected, mimicking those not working properly.

1 | INTRODUCTION

The upcoming fifth-generation (5G) mobile radio communications aims at providing higher bandwidth, more system capacity, and flexibility with the use of millimetre-wave frequencies [1]. Massive multiple input multiple output (MIMO) systems will fit in 5G scenarios [2], since they offer a large number of data streams, distributed to multiple users [3] and where the spectral efficiency can be optimized on a per user basis. To achieve higher spectral efficiency in terms of transmission, the radiated signal can be sent directly to the target using beamforming. This technique is widely used in MIMO systems, since it enables to transmit different power levels to different users [4] and, subsequently, the energy consumption may be reduced, accordingly. By adding more elements to a MIMO antenna array, the signal-to-noise ratio will increase due to the higher antenna gain, and hence, the possibility to achieve higher spectral efficiency. When the beamforming techniques are employed in MIMO antennas, the transmission becomes more efficient, since the signal can be transmitted directly to the target.

To perform beamforming, appropriate individual phase control of the radio signal that is fed to each antenna element is required to obtain the correct phase progression between elements, to produce constructive interference in far-field in the intended direction. For wireless communications, this advantage is further enhanced by using power amplifiers (PAs) with moderate output power to increase the overall dynamic range of the system and, thus, to enhance the radio the coverage. Nevertheless, this important technique presents some challenges, since the elements in antenna arrays are physically close to each other, and issues such as mutual coupling effects may arise [5].

Currently, there are several strategies to reduce/avoid the coupling effects that occur in antenna arrays. For instance, increasing the distance between elements without creating grating lobes is a simple approach to decrease signal coupling levels [6]. However, by doing so, the antenna array dimensions will increase significantly, which is not desirable for small-form system integration and rollout. Another aspect that results from increasing the distance between antenna elements is the higher side lobes that appear in the far-field, which may interfere with adjacent users [6].

The electromagnetic interactions between radiating elements present a significant impact on the system's performance, and they are more evident as the distance between the elements becomes smaller. When beamforming techniques are dynamically applied, the phase progression across the elements changes, and the coupling effects also do change accordingly. Besides the distance between the elements, the relative orientation of each element and the radiation characteristics will lead to several different behaviours. In this sense, when beamforming is performed (phase variation in each path), each antenna port is affected by its neighbouring elements, which changes the load presented to the PA. Consequently, in the presence of mutual coupling, the reflection coefficient for a single antenna element in an antenna array is called the active reflection coefficient (ARC) [7]. When all the antenna ports are excited simultaneously, the ARC is obtained [8] and the equivalent antenna model with uncoupled channels can be obtained [9]. Moreover, when the antenna performs beamforming, the ARC varies accordingly, which is a relevant coefficient to evaluate and predict how the PA will be affected when the beam is steered. When PAs are introduced before feeding the antenna elements without any sort of isolation, the coupling effects will interfere with the PAs' output power, linearity, efficiency, and so forth. Thus, these effects will degrade the PAs' performance and, consequently, the overall MIMO system performance. The higher the number of elements that composes an antenna array, the more these effects will contribute to decreasing the performance of MIMO systems in real scenarios. For this reason, specific understanding and characterization via coordinated measurements of the coupling phenomena become critical for effective overall system optimization.

The impact of coupling when beamforming is applied to MIMO systems is examined in [10], based on simulations. The authors concluded that mutual coupling effects should be considered in the analysis, design, and implementation of MIMO beamforming systems. When antennas are close to each other, the interference rejection and the signal tracking performance are degraded. Likewise, based on simulations, the authors in [11] show that mutual coupling originates individual PA compression phenomena and distorts the far-field information, which depends on the beam direction.

The theoretical concept of ARC has been proposed in [12] and [13]. In [14], the authors demonstrate ARC simulations in MIMO transmission antennas, showing the impact of the beam variation in the ARCs of the MIMO transmitting antenna. Besides, a framework to examine the impact of mutual coupling in the 2 × 2 MIMO system is presented in [15], where a full-wave electromagnetic antenna simulation with a path-based channel model is used to validate the method. Moreover, in [16] a method to obtain the active voltage standing wave ratio using the measurements of the ARC was proposed. This method requires dual directional coupler that measures both the incident and reflected waves to obtain the ARCs. In this case, to measure the ARCs of three antenna elements, the authors use a vector network analyzer (VNA), a power divider, and dual directional couplers. This means that the port 1 of the VNA is connected to the power divider and, then, the power divider outputs are connected to each dual directional coupler and, consequently, to the antenna element. By using this strategy, the system is not able to measure the impact of the beamforming in the antenna elements, since phase variations cannot be applicable in the VNA port 1. Furthermore, using the VNA to apply this method is a limitation because to measure ARC in antennas with a greater number of elements, it requires a VNA with higher number of port, which is economically expensive. In [17], a broadband characterization of multiport antennas is presented, where the total active reflection coefficient (TARC) is obtained. TARC is the square root of the available power produced by all excitations minus the radiated power, and then divided by the available power [17]. Furthermore, the ARC is not obtained and it is not detailed how the measurements were performed in terms of the measurement setup. The effect of mutual coupling on the ARC in phased array antennas with random layout is presented in [18], but based on simulations. In [19], a performance network analyser was used to evaluate the ARC, where two antenna elements were excited simultaneously. In this case, an expensive network analyzer was used and was limited by two ports, and beamforming performance was not considered. Also, by using simulations in [20] the authors demonstrate the active antenna impedance versus beam steering direction.

Therefore, the main goal of this study is to present a characterization system capable of measuring the ARCs in MIMO antennas, linear and planar, showing the impact of coupling, when beamforming is performed. When beamforming is applied in MIMO systems, the phase in each branch of the MIMO antenna varies, and a PA is connected to each element of the antenna, which will change the PA output impedance, degrading the entire MIMO system operation. Our novelty system allows measuring ARCs at once, since it excites all ports at the same time, unlike what happens with VNAs, to improve the MIMO system performance. In this sense, simulations will be conducted to anticipate the performance of the antenna when beamforming is performed. A suitable real-time and calibrated characterization system, based on low-cost software defined radios (SDR), will be used to perform the measurements of the linear and planar MIMO antennas. The proposed solution can be used to improve the design of PAs by taking into account load variations that are caused by beamforming coupling effects.

The article is organized as follows. In Section 2, the MIMO antenna arrays are described in detail. The characterization system is explained in Section 3, and the beamforming simulations are performed in Section 4. The experimental results obtained are presented in Section 5. Finally, in Section 6, conclusions will be drawn.

2 | MIMO ANTENNA ARRAY

A MIMO antenna was designed and optimized to operate at 2.587 GHz with Computer Simulation Technology (CST), with 14 elements, as represented in Figure 1. The interelement spacing of the antenna is $\lambda_0/2$, where λ_0 is the free-space wavelength. Each element is a square microstrip patch with an edge of 3 cm, as indicated in Figure 1, and the total dimension

of the antenna array is 39 cm × 11 cm. The MIMO antenna was built with Isola IS680 (h = 30 mil, Dk = 3.38) substrate, with a loss tangent of 0.0026 and fed by a coaxial probe method. The MIMO antenna consists of two rows, with seven elements in each row, where each antenna element is fed individually, as can be seen in Figure 2. Table 1 presents the MIMO antenna port number and its respective row (M) and column (N), inline to Figure 1. The reflection coefficient of each MIMO antenna element measured with the VNA is shown in Figure 3, demonstrating that the MIMO antenna elements are matched to 50 Ω at the operating frequency. The mutual coupling results measured in the VNA are presented in Figure 4 for both linear and planar configurations. As expected, the adjacent MIMO antenna elements present higher values of mutual coupling, highlighted with symbols. Moreover, the theoretical MIMO antenna radiation patterns for the linear and planar configurations are represented in Figure 5, when beamforming is applied for $\theta = 0°$, $\theta = 10°$, and $\theta = -10°$. From the simulations presented in Figure 5, it can be seen how the beam varies for those three angles. The main lobe and the side lobes are evident for both cases.

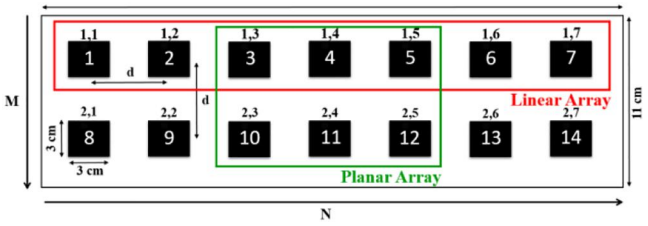

FIGURE 1 MIMO antenna array representation considering the linear and the planar arrays. MIMO, multiple input multiple output

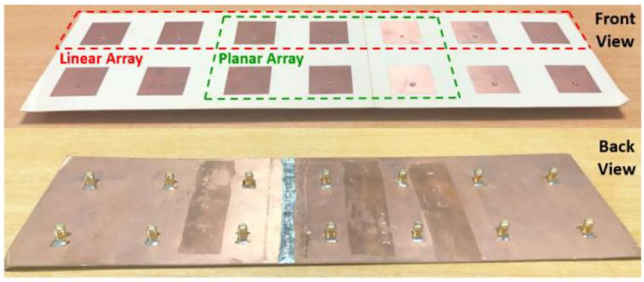

FIGURE 2 MIMO antenna array front and back view. MIMO, multiple input multiple output

TABLE 1 Multiple input multiple output antenna ports identification

M	1	1	1	1	1	1	1
N	1	2	3	4	5	6	7
Number of port	1	2	3	4	5	6	7
M	2	2	2	2	2	2	2
N	1	2	3	4	5	6	7
Number of port	8	9	10	11	12	13	14

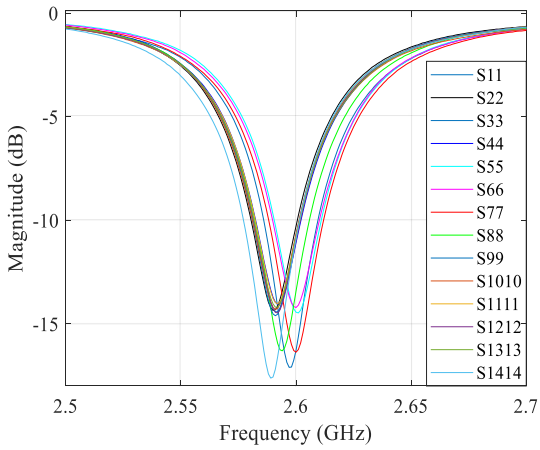

FIGURE 3 Magnitude of the reflection coefficient of each MIMO antenna element measured with a VNA for each port individually. MIMO, multiple input multiple output; VNA, vector network analyser

3 | CHARACTERIZATION SYSTEM

To measure the ARCs to evaluate the impact of mutual coupling in each antenna array element in the presence of real-time beamforming, when all the ports are fed simultaneously, an appropriate characterization system was designed, implemented, and optimized to perform a maximum of seven-port characterization at 2.587 GHz. The characterization system consists of a MIMO system composed of eight SDR Universal Software Radio Peripheral (USRPs) from National Instruments (NI USRP-2943R). Each USRP consists of one transmitter and two receivers, as shown in Figure 6(a). Additionally, each transmitter is connected to two directional couplers to separate the incident and reflected waves, which are acquired and processed by their respective receivers. Subsequently, the second coupler is connected to the MIMO antenna port.

3.1 | Calibration

Since the main goal is to perform real-time measurements when beamforming is executed, the characterization ports should be aligned and calibrated both in amplitude and phase. The characterization system, as mentioned previously, consists of several USRPs, and to perform real-time measurements, the sampling rate and the number of samples must be well defined to achieve high accuracy. In this regard, the characterization of the system itself was performed to obtain the maximum sample rate at which the system can operate with eight USRPs, without occurring phase mismatch between transmitters and receivers.

The calibration of the proposed system is performed in three stages, where an extra USRP is used as a reference. The first stage of the calibration process consists of connecting sequentially all the transmitters to the reference receiver and measuring their phase differences. The transmitters are then compensated to be aligned in phase. In the second stage of the calibration, the reference transmitter is connected sequentially

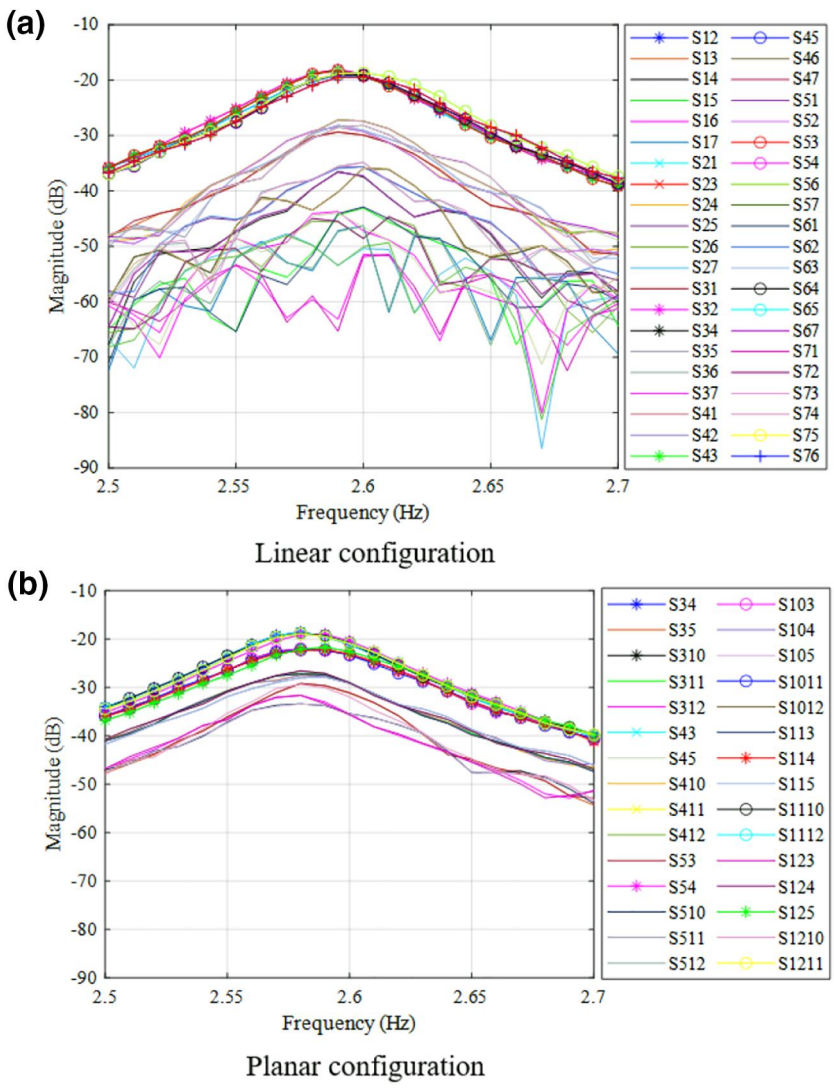

FIGURE 4 MIMO antenna mutual coupling results for linear and planar configuration: (a) linear configuration and (b) planar configuration. MIMO, multiple input multiple output

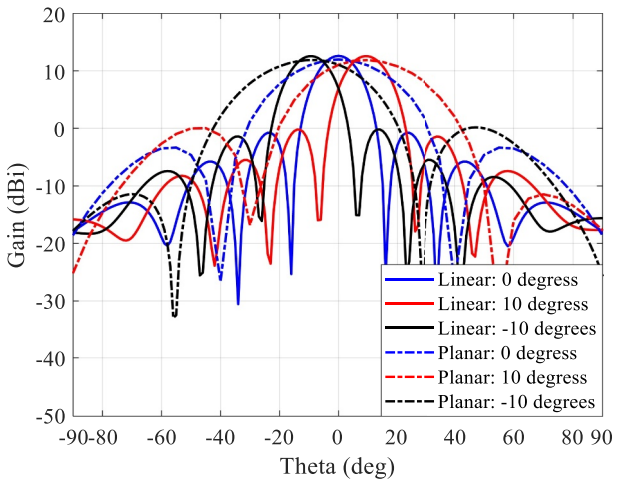

FIGURE 5 Simulated MIMO antenna radiation patterns for the linear and planar configuration, when beamforming is applied for 0°, 10°, and –10°. MIMO, multiple input multiple output

to the receivers to measure their phase and to align them in phase as well. The last stage of the calibration process is to apply a short, open, load (SOL) calibration to each port, based on the method presented in [21]. An additional power metre is used to calibrate the magnitude. As stated and demonstrated in [22], this method can be used in multiport measurements without the need for through ('thru') measurements.

3.2 | Algorithm

To execute the characterization system, a suitable algorithm was developed and illustrated in the block diagram of Figure 7. The first step of the algorithm is to select the carrier frequency and to insert the antenna specifications, such as the number of ports and the interelement spacing of the antenna, to obtain the antenna array factor (AF), for a selection of beamforming angles. In the second step of the algorithm, the transmitter and the receiver phases are

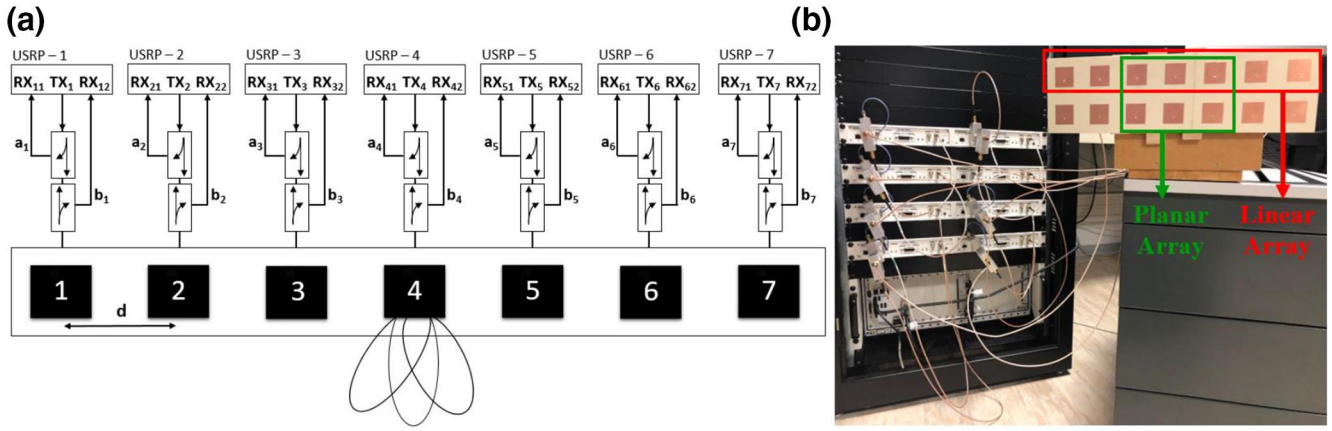

FIGURE 6 Characterization system: (a) block diagram and (b) measurement setup with the MIMO antenna. MIMO, multiple input multiple output

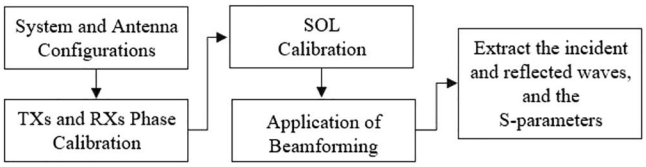

FIGURE 7 Algorithm block diagram

calibrated, as explained in the previous subsection. The SOL calibration is carried out in the third step of the algorithm, and its procedure can be found in the previous subsection as well. The last step of the algorithm is the computation of beamforming excitation vector, taking into account the AF for the type of antenna to be characterized (linear or planar), the number of ports and the antenna specifications, as indicated in the first step of the algorithm.

For each beam angle (which was defined by the user), the algorithm calculates the required phase (by using the AF) to apply in each antenna element. Then, the incident and the reflected waves of each port are obtained and the ARCs are acquired at once in each port. In the end, the results of each measurement are saved in files. In summary, the proposed characterization system behaves as a real-time N-port VNA, but with the addition of having all the ports are excited at the same time and allowing to change the phase of each port.

4 | BEAMFORMING SIMULATION RESULTS

The main purpose of the beamforming techniques is to transmit a signal directly to a target, instead of spreading the signal to an entire area. Consequently, to control the MIMO antenna beam direction, the excitation vector must be computed. To calculate the beam direction, the expression of the AF [23] is used, which represents the radiation pattern of an antenna array. To this extent, for a linear and uniform element distribution, the phase required to provide a beam in the θ_p direction (with respect to the broadside direction) is given by

$$\psi(n) = n \cdot k \cdot d \cdot \cos\theta_p, k = \frac{2\pi}{\lambda} \quad (1)$$

where d is the interelement spacing, k is the wavenumber in free space, and n is the index of the element within its respective columns as shown in Figure 1. In this case, $m = 1$ since m represents the index of rows. Furthermore, considering a planar array, where the elements are placed in a rectangular or in a planar grid, the phase required to provide a beam in the (θ_p, φ_p) direction is given by (2)

$$\psi(m,n) = k \cdot d \cdot m \cdot \sin\theta_p \cdot \cos\phi_p + k \cdot d \cdot n \cdot \sin\theta_p \cdot \sin\phi_p \quad (2)$$

where m is the element index within its respective rows as shown in Figure 1. To predict how the MIMO antenna will behave when beamforming is applied, several simulations were performed considering a sweep of θ_p from –90° to 90°. In MATLAB, the incident waves, $a(m,n)$, for each port were calculated based on (3):

$$a_{(m,n)} = A \cdot \exp^{j\psi(m,n)} \quad (3)$$

where A is the amplitude of the signal. As mentioned previously, the MIMO antenna was characterized with a VNA, individually. Then, the S-parameters were extracted and they were loaded to the MATLAB to compute the reflected waves plus any coupling effect generated by the other elements, $b(m, n)$, for each port with indexes (m,n) as follows:

$$b(m,n) = \sum_{k=1}^{K} a_k \cdot S_{(m,n)k} \quad (4)$$

where K is the maximum number of ports to characterize, (m,n) is the number of the port, a_k is the incident wave of each

port, m represents rows, and n represents columns, as depicted in Figure 1. It should be noted that for the linear case, $m = 1$. K is the maximum number of ports to characterize, $K = M*N$, which in this case is 14, since the MIMO antenna is composed of two rows ($M = 2$) and seven columns ($N = 7$). Note that (m, n) represents the index of the MIMO antenna port, as shown in Figure 1 and Table 1. After that, the ARC for each port was calculated based on

$$\Gamma_{(m,n)(m,n)} = \sum_{k=1}^{K} \frac{a_k \cdot S_{(m,n)k}}{a_{(m,n)}} = \frac{S_{(m,n)1} \cdot a_1 + S_{(m,n)2} \cdot a_2 + \ldots + S_{(m,n)k} \cdot a_k}{a_{(m,n)}} \quad (5)$$

Considering (5), the calculation of the ARC, in each port, takes into account the impact of the coupling generated by adjacent antenna elements. The resulting simulation for the linear MIMO antenna is shown in Figure 8 (red line). Note that only seven elements from the upper row were considered (linear case, refer to Figure 1). The remaining elements were connected to a 50-Ω load. Besides, the MIMO antenna elements are identified in Figure 1. Moreover, Figure 8 indicates the trajectories of the beam steering angles, where positive angles are in blue and negative angles are in green.

The same procedure was performed for the planar MIMO antenna, where six elements of the antenna, as shown in Figure 1, were considered. The beamforming was performed for the same values of θ and $\varphi = 0°$ (only azimuth beamforming). The simulation results for the planar antenna are depicted in Figure 9 (red line). The trajectories of the beam steering angles in Figure 9 are presented, where positive angles are in blue and negative angles are in green. From these two simulations, linear and planar, it can be concluded that the elements on the edges of the antenna are less affected by adjacent elements, as their resulting pattern resembles a communication system with a strong narrowband interferer. On the other hand, the elements that are in the middle of the array exhibit a pattern that results from the contributions of neighbouring elements.

By performing these two simulations, it can be estimated how the antenna will behave in the presence of beamforming.

5 | CHARACTERIZATION WITH THE PROPOSED SYSTEM

The characterization system was used to perform the beamforming measurements on the linear and planar MIMO antennas, which operates at a frequency of 2.587 GHz. To apply the beamforming in the linear and planar MIMO antennas, the excitation vector was computed based on the AF for these two approaches to generate beams from –90° to +90°, with a step of 5°, similar to the simulations presented in the previous section. To validate that the linear and planar MIMO antennas are varying the beam accordingly, a single patch receiving antenna built on Isola IS680 (h = 30 mil, Dk = 3.38) substrate, tuned to 2.587 GHz, was introduced into the setup and placed in the far-field region. This antenna was placed in front of the transmitting MIMO antenna, in far-field, and connected to a USRP receiver. The beam was varied from –90° to +90°, while the receiving antenna was kept fixed. The received power of the linear and planar MIMO antennas are depicted in Figure 10, demonstrating that the beam is operating as expected.

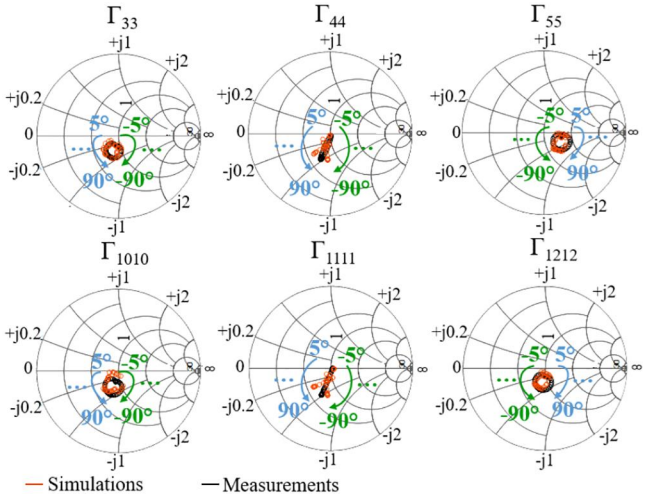

FIGURE 9 ARCs of planar MIMO antenna when beamforming is performed. In red simulations by using the S-parameters extracted from VNA, and, in black, measurements using the proposed characterization system. ARC, active reflection coefficient; MIMO, multiple input multiple output; VNA, vector network analyzer

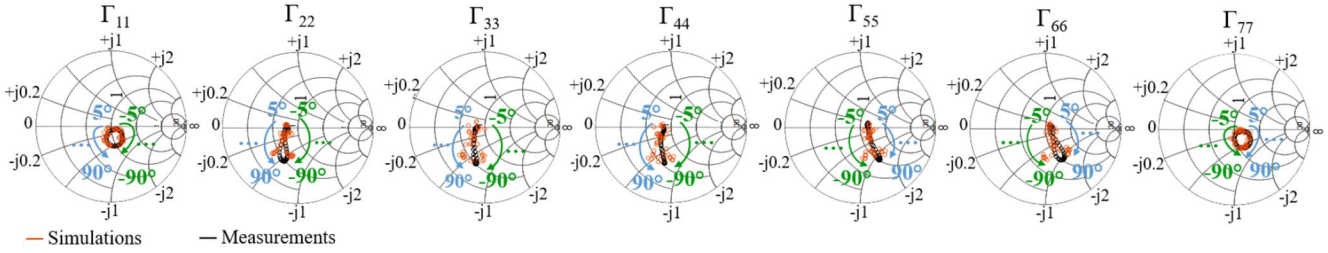

FIGURE 8 ARCs of linear MIMO antenna when beamforming is performed. In red simulations by using the S-parameters extracted from VNA, and, in black, measurements using the proposed characterization system. ARC, active reflection coefficient; MIMO, multiple input multiple output; VNA, vector network analyzer

The coupling effects are the absorption of the energy that was radiated by the other elements and the antenna elements can be evaluated in terms of incident and reflected waves. In this sense, the beamforming was executed for linear and planar MIMO antennas. Then, the magnitude of the ARCs for each antenna element, when the beamforming is performed for a sweep of θ from –90° to +90°, was obtained. The results are presented in Figure 11, for the linear and the planar MIMO antennas (with $\varphi = 0°$). It is evident from the analysis of both images that the beam variation leads to large variations in the ARC of the antenna, which depends on the angle. Moreover, it can be seen that the antenna elements placed in edges are more affected by the coupling when the beam is steered. Besides, the ARC results are acceptable, since the magnitude results are below 10 db for –45° and +45°. To understand the impact of beamforming in each antenna element, the ARC of each antenna element is represented on a Smith chart. For the linear MIMO antenna, the results are superimposed on the simulation results represented in Figure 8 (simulations with a red line and experimental results with a black line), while Figure 9 also shows the results for the planar MIMO antenna. It can be concluded that the elements in the middle of the antenna present a different behaviour of the edge elements, as expected from the simulated results. These two measurements (linear and planar) indicate a slight difference compared to simulations, especially with the elements that are not at the edges of the antenna array.

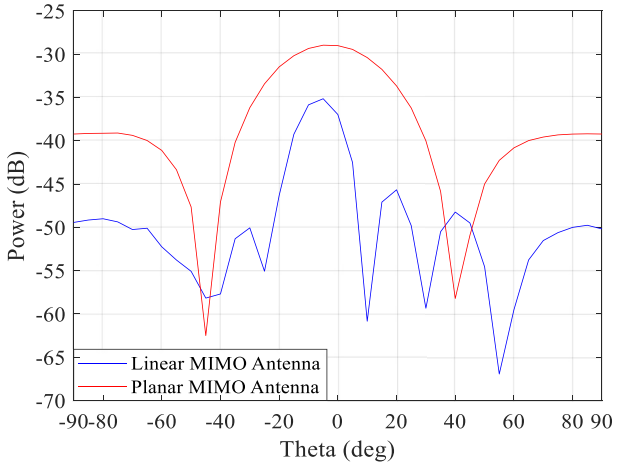

FIGURE 10 Far-field received power patterns for the linear and planar MIMO antennas. MIMO, multiple input multiple output

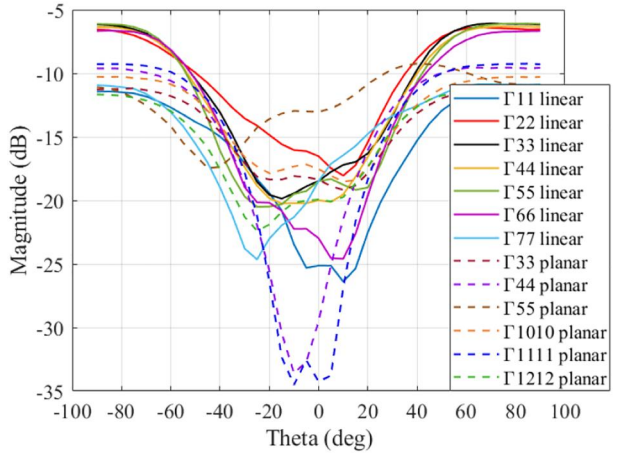

FIGURE 11 ARC of MIMO antenna, considering the linear and the planar array, measured using the characterization system, when beamforming is performed. ARC, active reflection coefficient; MIMO, multiple input multiple output

In order to show that multipath effects have a no negligible contribution, a metal plane was intentionally positioned in front of the antenna transmitter to assess its impact on each port of the antenna. As demonstrated in Figure 12, for the linear MIMO antennas, and in Figure 13, for the planar MIMO antenna, the ARC of each port, when compared with the initial measurements, changed significantly. In this real-time experiment, by using this characterization system, the impact of a multipath environment, when beamforming is applied, is demonstrated, which is important since this affects the antenna and, consequently, the entire MIMO system performance. Therefore, when beamforming is applied in real time, the mutual coupling phenomena is different from those expected, which will interfere with the performance of the PAs that are placed before each antenna element, degrading the entire MIMO system performance. Consequently, this type of measurement is of utter importance to improve the performance of MIMO systems.

Finally, two additional experiments were conducted. In one of those final experiments, the element of the middle of the linear MIMO antenna was intentionally disconnected and terminated with a 50 Ω load. The aim was to simulate a scenario where one of the antenna elements is damaged to evaluate the impact of the coupling on the remaining elements. The ARC results of this experiment are shown in Figure 14, where it is clear that the neighbouring elements radically change their pattern. From this comparison, it is observed that

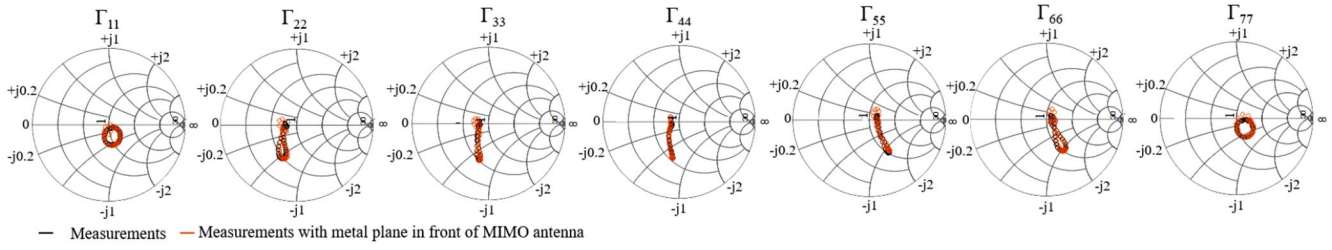

FIGURE 12 ARC comparison between measurements performed with and without a metal plane in front of linear MIMO antenna, when beamforming is performed. ARC, active reflection coefficient; MIMO, multiple input multiple output

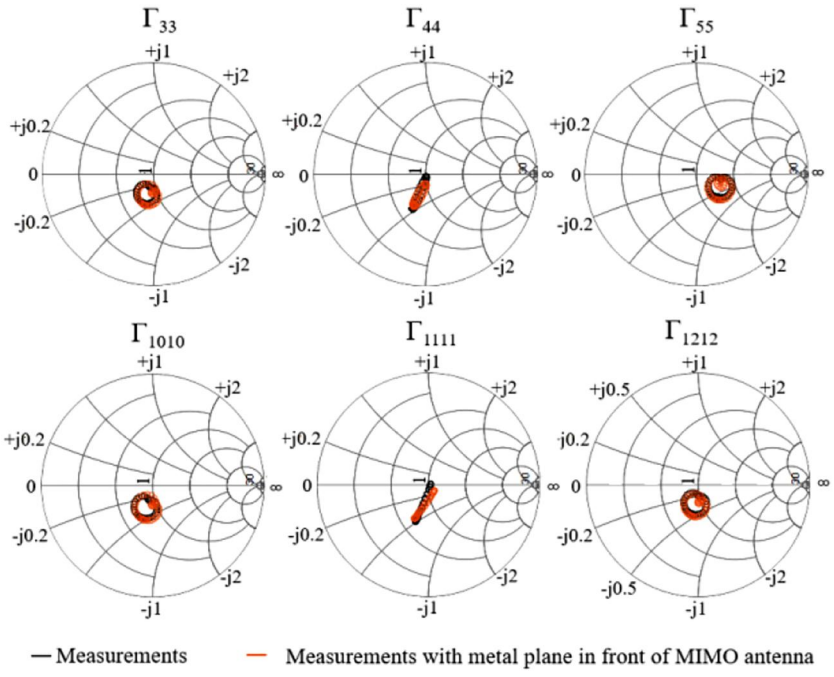

FIGURE 13 ARC comparison between measurements performed with and without a metal plane in front of planar MIMO antenna, when beamforming is performed. ARC, active reflection coefficient; MIMO, multiple input multiple output

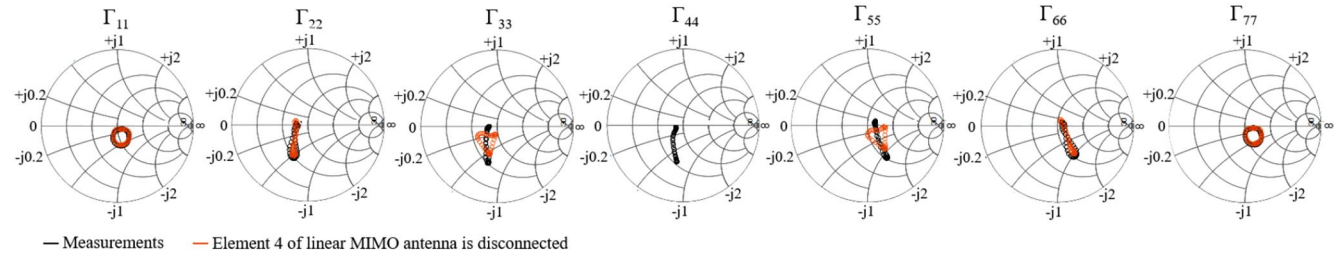

FIGURE 14 ARC comparison between measurements when the fourth element is operating and when is disconnected from the linear MIMO antenna, when beamforming is performed. ARC, active reflection coefficient; MIMO, multiple input multiple output

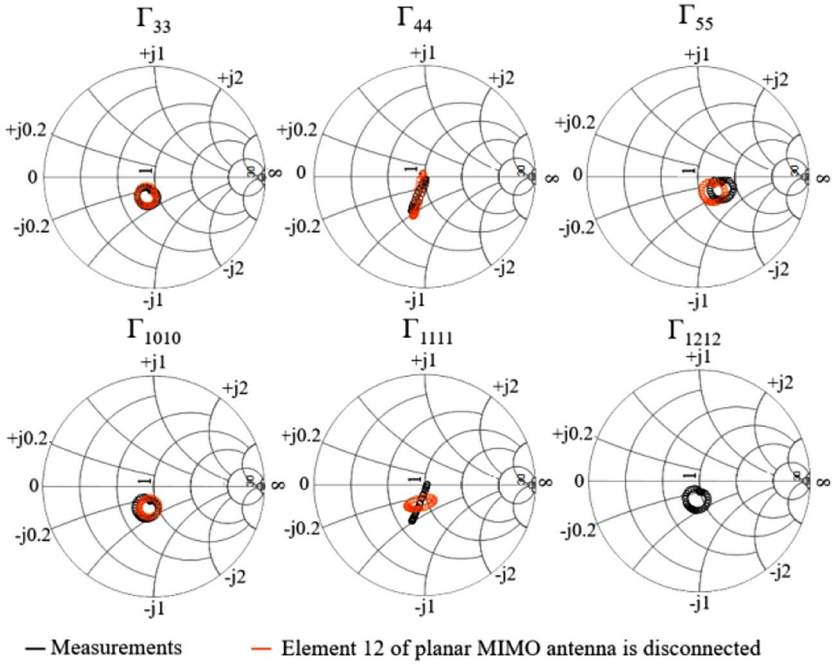

FIGURE 15 ARC comparison between measurements when the 12th element is operating and when is disconnected from the planar MIMO antenna, when beamforming is performed. ARC, active reflection coefficient; MIMO, multiple input multiple output

the elements that are next to the fourth element are the ones that present a higher variation in terms of the mutual coupling (elements 3 and 5). The same procedure was performed for the planar array, and the results are shown in Figure 15. In this case, one of the elements of the edge was disconnected (element 12). In this situation, the neighbouring element also totally changed its pattern. These experiments were carried out to obtain information about the behaviour of the entire antenna when one of the elements is damaged since it is a situation that can occur in a real scenario and affects the entire system performance.

6 | CONCLUSION

In this study, a real-time beamforming characterization system designed to evaluate the coupling effects and extract the ARCs in MIMO antenna was presented. The system provides the flexibility to perform measurements of the incident and reflected waves of each port by exciting each port at once.

Simulations to predict these effects were carried out by using S-parameters extracted with a VNA. The characterization of linear and planar MIMO antennas was accomplished, demonstrating the impact of real-time beamforming on each antenna element. It is shown that intentionally adding or approaching reflection objects may cause noticeable changes since this shows their impact when the antenna is performing beamforming. Moreover, the impact of a damaged antenna element was also shown to demonstrate the influence in each port of the MIMO linear and planar antennas. When connecting PAs to the antenna elements, the information about the load changes is important because when one antenna element is damaged, the performance of the remaining elements and PAs are also degraded, and the overall antenna operation may not be sufficient to keep the MIMO system operating with acceptable efficiency. In terms of algorithm limitations, this one was designed for a maximum of seven ports, since it is the maximum number of ports in our characterization system. However, this limitation is easily overcome, since more transmitters and receivers can easily be integrated to have a more generic algorithm solution.

This characterization system can be used to extract ARCs from MIMO antenna arrays when beamforming is performed, which is useful to improve the MIMO systems' performance. With the knowledge of the static coupling/reflections, the presented work may be relevant to optimize and boost the efficiency of future 5G systems.

ACKNOWLEDGEMENTS

This work is supported by the European Regional Development Fund through the Competitiveness and Internationalization Operational Program, Regional Operation Program of Lisbon, Regional Operational Program of the Algarve, in component FEDER, and the Foundation for Science and Technology, Project, RETIOT, POCI-01-0145-FEDER-016432. The work of Marina Jordão was supported by the Fundação para a Ciência e Tecnologia (F.C.T.) through Fundo Social Europeu (FSE) and by Programa Operacional Regional do Centro under Ph.D. Grant SFRH/BD/143204/2019. The work of Daniel Belo was supported by the Fundação para a Ciência e Tecnologia (F.C.T.) under Ph.D. Grant SFRH/BD/142403/2018. This work was sponsored in part by the Roger Pollard Student Fellowship from the Automatic RF Techniques Group.

ORCID

Marina Jordão https://orcid.org/0000-0001-5791-4602
Rafael F. S. Caldeirinha https://orcid.org/0000-0003-0297-7870

REFERENCES

1. Kotterman, W.A.T., et al.: New challenges in over-the-air testing. In: 2017 11th European Conference on Antennas and Propagation (EUCAP), Paris, pp. 3676–3678 (2017)
2. Chen, W.K.: Linear Networks and Systems. Wadsworth, Belmont, CA pp. 123–135.(1993)
3. Balanis, C.:Ioannides, P. I.: Synthesis Lectures on Antennas. Introduction to smart antennas, vol. 5, pp. 1–179. Morgan and Clay-pool Publishers (2007). https://doi.org/10.2200/S00079ED1V01Y200612ANT005
4. Gustafsson, M., et al.: Impact of mutual coupling on capacity in large MIMO antenna arrays. In: The 8th European Conference on Antennas and Propagation (EuCAP 2014), The Hague, pp. 2723–2727 (2014)
5. Kottkamp, M., Rowell, C.: Antenna Array Testing—Conducted and Over the Air: The Way to 5G. Rohde & Schwarz White Paper (2016)
6. Rusek, F., et al.: Scaling up MIMO: opportunities and challenges with very large arrays. IEEE Signal Process. Mag. 30(1), 40–60 (2013)
7. Mailloux, R.J.: Phased Array Antenna Handbook. Artech House, Boston, MA (2005)
8. Kahn, W.: Active reflection coefficient and element efficiency in arbitrary antenna arrays. IEEE Trans. Antennas Propag. 17(5), 653–654 (1969)
9. García-Muñoz, L.E., et al.: Broadband active differential array for the mid-frequency SKA band. IEEE Antennas Propag. Mag. 56(2), 27–38 (2014)
10. Zheng, Z., et al.: Robust adaptive beamforming against mutual coupling based on mutual coupling coefficients estimation. IEEE Trans. Veh. Technol. 66(10), 9124–9133 (2017)
11. Hefnawi, M., Gai, J., Elasoued, R.A.: Mutual coupling effects on mimo-adaptive beamforming systems. In: International Conference on Networking and Services (ICNS'07), Athens, p. 106 (2007)
12. Pozar, D.M.: The active element pattern. IEEE Trans. Antennas Propag. 42(8) (1994)
13. Pozar, D.M.: A relation between the active input impedance and the active element pattern of a phased array. IEEE Trans. Antennas Propag. 51(9) (2003)
14. Savy, L., Lesturgie, M.: Coupling effects in MIMO phased array. In: 2016 IEEE Radar Conference (RadarConf), Philadelphia, PA, pp. 1–6 (2016)
15. Wallace, J.W., Jensen, M.A.: Mutual coupling in MIMO wireless systems: a rigorous network theory analysis. IEEE Trans. Wirel. Commun. 3(4), 1317–1325 (2004)
16. Colon-Diaz, N., et al.: Measurement of active reflection coefficient for co-located MIMO radar using dual directional couplers. In: 2018 AMTA Proceedings, Williamsburg, VA, pp. 1–4 (2018)
17. Manteghi, M., Rahmat-Samii, Y.: Broadband characterization of the total active reflection coefficient of multiport antennas IEEE Antenn. Propag. Soc. Int. Sympos. Digest. 3, 20–23 (2003)
18. de Lera Acedo, E., et al.: On the effects of mutual coupling in the active reflection coefficient of wide-field scanning electrically large random phased arrays. In: 2016 International Conference on Electro-

magnetics in Advanced Applications (ICEAA), Cairns, QLD, pp. 683–685 (2016)
19. Vilas Boas, E.C., et al.: Dual-band switched-beam antenna array for MIMO systems. IET Microw. Antennas Propag. 14(1), 82–87 (2020)
20. Fager, C., et al.: Analysis of nonlinear distortion in phased array transmitters. In: 2017 Integrated Nonlinear Microwave and Millimetre-wave Circuits Workshop (INMMiC), Graz, pp. 1–4 (2017)
21. Jordão, M., et al.: Characterization of electromagnetic coupling effects in MIMO antenna array beamforming. In: 2019 IEEE MTT-S International Microwave Symposium (IMS), Boston (2019)
22. Heuermann, H.: Calibration of network analyzer without a thru connection for non-linear and multiport measurements. IEEE Trans. Microw. Theory Technol. 56(11), 2505–2510 (2008)
23. Zooghby, A.E.: Smart Antenna Engineering, 1st ed. Artech House, Inc (2005)

How to cite this article: Jordão M, Belo D, Caldeirinha RFS, Oliveira ASR, Carvalho NB. Active reflection coefficients characterization system for multiple input multiple output antennas. *IET Microw. Antennas Propag.* 2021;15:511–520. https://doi.org/10.1049/mia2.12078